crystals

MDPI

Article

Phase Transition of Nb_3Sn during the Heat Treatment of Precursors after Mechanical Alloying

Wanshuo Sun [1,2] and Shunzhong Chen [1,2,*]

[1] Institute of Electrical Engineering, Chinese Academy of Sciences, Beijing 100190, China; sunwanshuo@mail.iee.ac.cn
[2] University of Chinese Academy of Sciences, Beijing 100049, China
* Correspondence: chenshunzhong@mail.iee.ac.cn

Abstract: The phase transition process of Nb_3Sn during heat treatment exerts important influences on Nb_3Sn formation and the superconducting characteristics of Nb_3Sn superconductors. A simple method for quickly preparing Nb_3Sn was studied. First, Nb, Sn, and Cu powders were mechanically alloyed to prepare the precursor. Then, the precursor was heat treated at different times to form Nb_3Sn. During the first stage, the morphology and crystal structure of the products were analyzed after different milling times. The results of the transmission electron microscopy showed the poor crystallinity of the products compared with the original materials. During the second stage, heat treatment was performed at different temperatures ranging from room temperature to 1073 K. After treatment, the products were studied via X-ray diffraction analysis to determine how the structure changed with increasing temperature. Only the Nb diffraction peaks in the precursor were observed after high-energy ball milling for more than 3 h. When the heat treatment temperature was above 773 K and heat treatment time was 15 min, Nb_3Sn began to form. When the temperature was above 973 K, some impurities, such as Nb_2O_5, appeared. After 5 h of ball milling, the precursor was heat treated at different times in a vacuum heat treatment furnace. The crystal structure of the product exhibited evident diffraction peaks of Nb_3Sn. The critical temperatures of the samples that were heat treated at different times were between 17 K and 18 K. The magnetic critical current density of the sample versus the applied magnetic field at 4.2 K indicated that the magnetic J_c was approximately 30,000 A/cm^2.

Keywords: Nb_3Sn; superconducting characteristics; phase transition; mechanical alloying

check for updates

Citation: Sun, W.; Chen, S. Phase Transition of Nb_3Sn during the Heat Treatment of Precursors after Mechanical Alloying. *Crystals* **2023**, *13*, 660. https://doi.org/10.3390/cryst13040660

Academic Editors: Daniel Medyński, Grzegorz Lesiuk and Anna Burduk

Received: 24 February 2023
Revised: 28 March 2023
Accepted: 9 April 2023
Published: 11 April 2023

Copyright: © 2023 by the authors. Licensee MDPI, Basel, Switzerland. This article is an open access article distributed under the terms and conditions of the Creative Commons Attribution (CC BY) license (https://creativecommons.org/licenses/by/4.0/).

1. Introduction

Since Nb_3Sn was discovered by Matthias in 1954 [1], research on this compound has elicited considerable attention, particularly regarding its preparation and superconductive characteristics. Compared with NbTi, Nb_3Sn has higher critical temperature (above 18 K) and critical magnetic field of around 30 T. Nb_3Sn superconductors have important applications in high magnetic field situations, particularly at above 10 T. Current applications of Nb_3Sn include magnetic resonance imaging [2], nuclear magnetic resonance [3], dipole and quadrupole magnets for particle accelerators, and other areas where high magnetic fields are required, such as the International Thermonuclear Experimental Reactor [4]. Conventional manufacturing methods, such as bronze technology [5,6], internal tin technology [7], and powder-in-tube [8,9] process, require a long period of heat treatment at around 650 °C to allow Sn to react with Nb and form Nb_3Sn superconductors. These methods are time consuming, and their costs are high.

Heat treatment is a key point in the preparation of Nb_3Sn. Heat treatment temperature exerts an important effect on the upper critical field B_{c2}, with a higher reaction temperature leading to higher B_{c2} [10]. Many studies on heat treatment have investigated the influences of temperature variation, heat treatment time, temperature gradient, ascending temperature

speed, and temperature uniformity on the superconducting characteristics of Nb_3Sn [11]. Various factors that are required to form fine and homogeneous grains of Nb_3Sn were studied through a series of experiments [12,13]. The phase transformations of high J_c Nb_3Sn strands during reaction heat treatment were studied by performing synchrotron X-ray diffraction (XRD) measurements.

The amount of Sn plays an important role in the superconducting properties of Nb_3Sn. The critical temperature sharply increases from approximately 6 K to approximately 18 K when the percentage of Sn is increased from below 20% to above 24.5%. For some superconductors in which Sn concentration is insufficient or some regions with a deficient stoichiometric ratio of Sn, the critical temperature of Nb_3Sn may be below 9 K [14]. The upper critical field is also affected by the amount of Sn in accordance with the Werthamer–Helfand–Hohenberg theory. Therefore, increasing the amount of Sn or making the stoichiometry of the Nb_3Sn layer more uniform is important to increase the upper critical field and the critical temperature [4]. The addition of Cu can decrease A15 formation temperature and obtain Nb_3Sn grains with small sizes by limiting grain growth. Thus, higher grain boundary density can be obtained to improve the bulk pinning force [15]. A typical reaction scheme for high-performance Nb_3Sn conductors is increasing the temperature to 483 K and holding this temperature for 100 h, ramping the temperature to 673 K and holding this temperature for 50 h, and then ramping to the final reaction temperature (923–973 K) and holding this temperature for a long period (50–200 h). The heat treatment of the Nb_3Sn bulk is equally important because the bulk can be used to fabricate the Nb_3Sn superconducting joint, which must be heat treated with Nb_3Sn conductors. Reducing the length of the final heat treatment process is significant for Nb_3Sn magnet production.

We report a simple and time-saving synthesis technique for Nb_3Sn that proceeds through a mechanical alloying method, followed by short-term heat treatment. Nb, Sn, and Cu powders were mixed and alloyed through mechanical alloying, and the precursors were synthesized via high-energy ball milling of the as-blended powders. Then, the precursors were heat treated to form Nb_3Sn. However, before Nb_3Sn nucleation and growth, other intermetallic phases were synthesized during the large temperature intervals. These phases affected the final reaction in the formation of Nb_3Sn. The influence of temperature variation on Nb_3Sn reaction was studied, and changes in crystal structure with temperature were measured to study the change in phase transition during the process. After high-energy ball milling at different times, the precursors were prepared and heat treated at various temperatures ranging from 298 K to 1073 K at 10–50 K intervals.

2. Experiment

All original materials used in this work, including Nb, Sn, and Cu, were composed of 99.9% pure powder, which were 5–20 μm in scale. Nb, Sn, and Cu were blended with a molar ratio of 3:1:1. Then, the blended powders were placed in a ball mill tank. The rotational speed of the ball mill was 1725 rpm. The precursors were synthesized after high-energy ball milling. The procedure above was performed in a glove box to prevent the blended powders from oxidizing in a high-temperature and high-pressure environment. The as-blended powders were mechanical alloyed at different times by using a Spex 8000D mixer. The prepared precursors were then heat treated from room temperature to 1073 K. During the process, we studied the changes in the crystal structure of the precursors after the selected temperatures, which was approximately at every 50 K interval from 298 K to 873 K and from 973 K to 1073 K and at every 10 K interval from 903 K to 953 K. The heating rate was 10 K per minute, and sintering holding time was 15 min at each sintering temperature point.

The morphology of the product was recorded using a scanning electron microscope. A transmission electron microscope was used to analyze the crystallinity of the as-prepared samples. The prepared samples were characterized via XRD on an Empyrean X-ray diffractometer. The temperature dependence of magnetizability was measured using a physical property measurement system (PPMS-9).

3. Results and Discussion

Figure 1 shows the scanning electron microscopy (SEM) images of the original samples. Figure 2 shows the SEM images and the energy-dispersive X-ray spectroscopy (EDS) mapping images of the products after the milling of Nb–Sn–Cu powders for 5 h. The images indicated that all the elements were homogeneously dispersed. Patankar [16] reported that brittle Nb with a body-centered cubic structure is likely to get fragmented and get coated onto the surface of ductile Sn. Patankar believed that the depth of XRD was insufficient to penetrate the Nb shell. Thus, Sn was not observed from the XRD result. However, the results of the EDS mapping images showed that Sn and Cu were homogeneously dispersed around Nb and did not exhibit the core–shell structure. This phenomenon may be attributed to the amorphization of Sn with increasing milling time. The original material was several microns in size. After mechanical alloying, the dimensions of the particles decreased. Even nanocrystalline materials were formed due to high-energy ball milling.

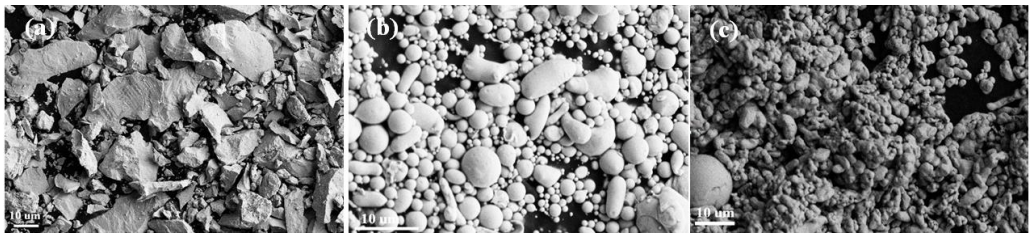


Figure 1. SEM images of original samples: (**a**) Nb, (**b**) Sn, and (**c**) Cu.

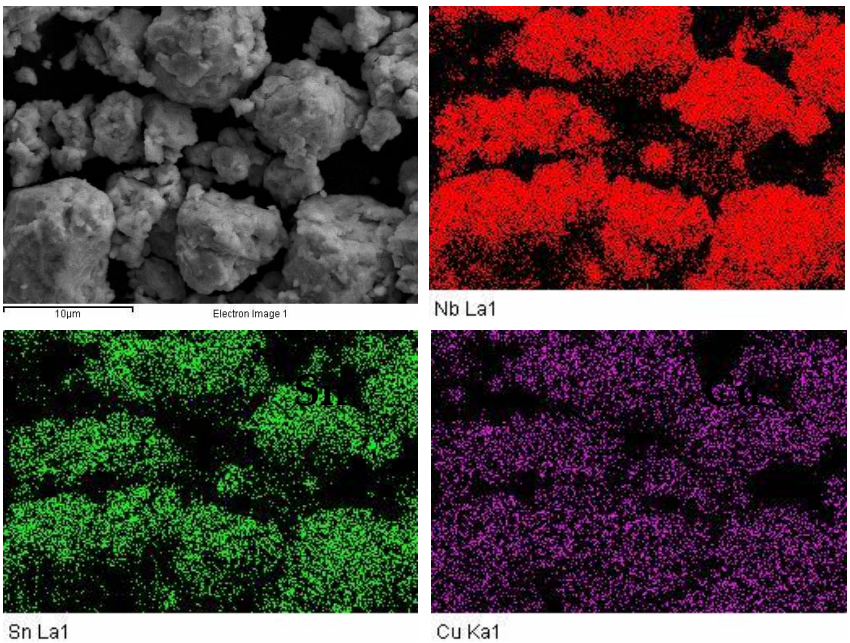


Figure 2. SEM image and EDS mapping of the samples after the milling of the Nb–Sn–Cu powder for 5 h.

Figure 3 depicts the elemental composition of the as-blended particles after mechanical alloying, as illustrated in the inset of the figure. From the results of the selected area with a few microns, Nb, Sn, and Cu were included and mixed in stoichiometric ratio, indicating that a new combination of elements was constructed at the microscopic level. This finding exerted a significant effect on the reaction of Nb with Sn to produce Nb_3Sn due to the microscopic stoichiometric ratio and the closer diffusion distance between Nb and Sn in the subsequent heat treatment process.

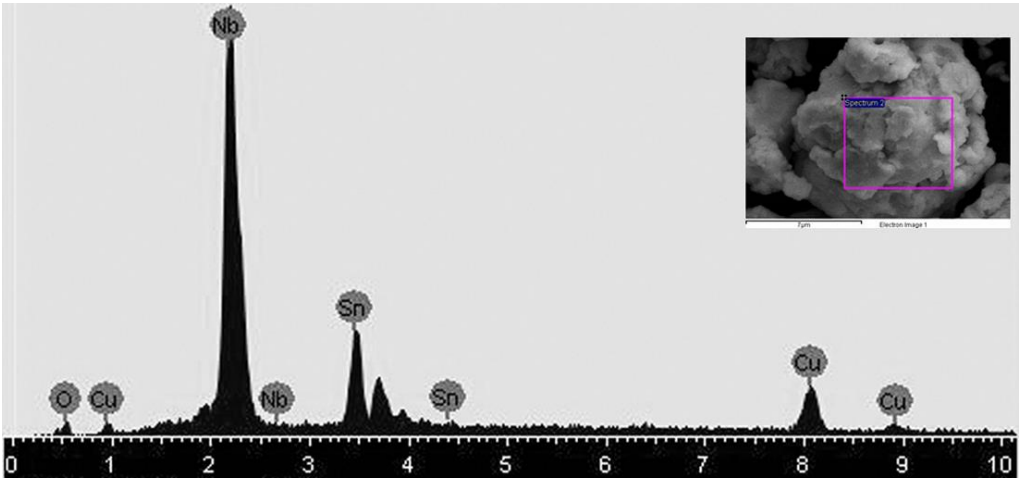


Figure 3. EDS analysis of the sample after the milling of the Nb–Sn–Cu powder for 5 h.

Figure 4 shows the typical low-magnification and high-resolution transmission electron microscopy (TEM) micrographs of the samples. The selected area electron diffraction pattern shown in the inset of Figure 4a suggested that the products exhibited poor crystallinity after ball milling for 5 h. One study suggested that Sn transformed into the amorphous phase because Nb and Cu were harder than Sn [17]. Some diffraction spots were observed with halo rings in the figure. The Nb grains were confirmed through the high-magnification micrograph in Figure 4b.

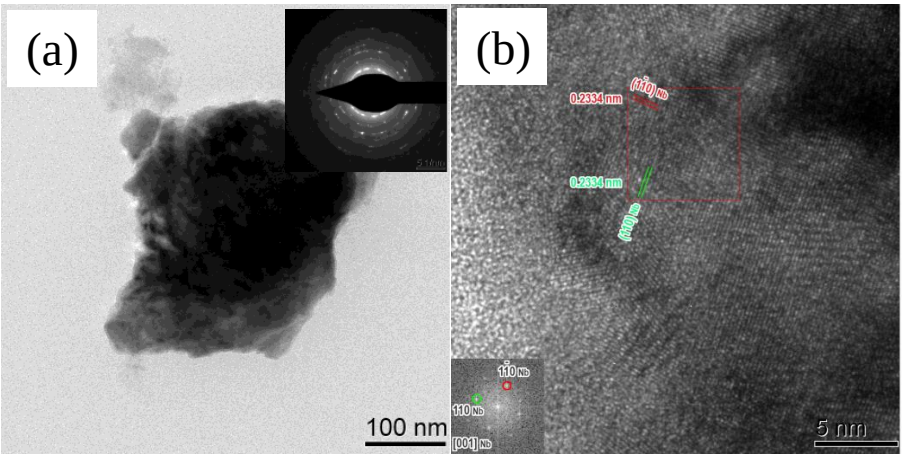


Figure 4. TEM micrograph of the sample: (**a**) low-magnification micrograph and (**b**) high-magnification micrograph.

The finding was consistent with the XRD result below. Diffraction intensity became weaker with increasing milling time. This result suggested that on the one hand, the crystalline grain size of products became smaller and even reached nanometer scale, broadening the width of diffraction peaks. On the other hand, the high-energy ball milling introduced many defects into the products. The disorder degree of interfacial atoms increased considerably, reducing diffraction intensity. The high-resolution TEM micrograph showed the interplanar crystal spacing of Nb.

Figure 5 presents the XRD patterns of the particles after mechanical alloying at different times. The results showed that the diffraction peaks of Sn and Cu disappeared when milling time reached 1 h compared with the apparent diffraction peaks of the original as-milled particles. The intensity of peaks decreased with increasing milling time. When ball milling time reached 10 h, the primary diffraction peak of Nb evidently broadened compared with the initial stage. High-energy mechanical alloying caused the continuous cold welding and

fracturing of different particles. Grain size decreased with increasing milling time. The results showed that the effects of ball milling on the crystallinity of products became worse with increasing milling time. This effect was also observed from the TEM results of the products. Simultaneously, long-range-order parameters decreased with increasing milling time due to the large number of defects and the high amount of grain boundary energy during high-energy mechanical alloying. Both caused the intensity of peaks to decrease and transform into metastable phases.

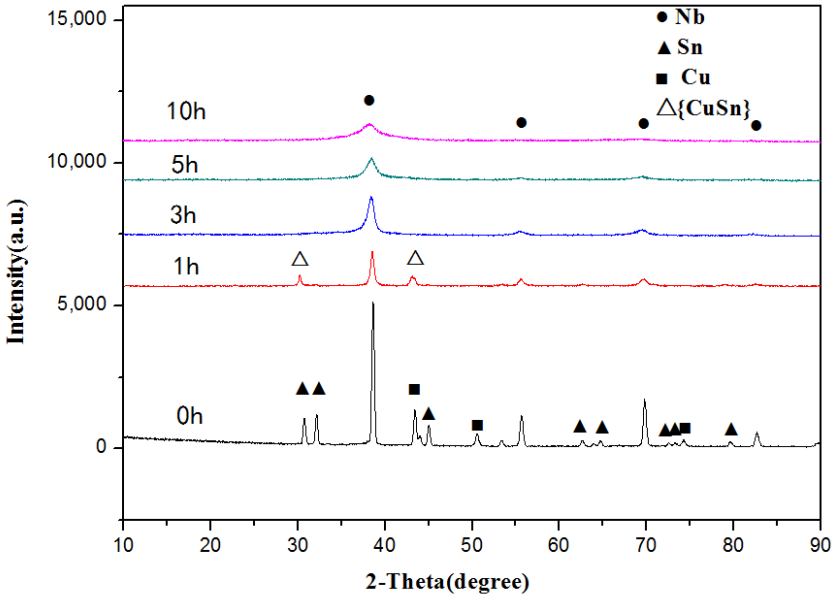


Figure 5. XRD patterns of the particles after mechanical alloying at different times.

Figure 6 presents the XRD patterns of the products after different heat treatment temperatures ranging from 298 K to 573 K. These curves represent the crystal structures of the products after each heat treatment at different temperatures. As shown in the figure, the XRD pattern at 298 K presents the measurement result at room temperature, i.e., the crystal structure of the sample after mechanical alloying. Only the Nb diffraction peaks are shown. The Sn and Cu diffraction peaks disappeared after high-energy mechanical alloying.

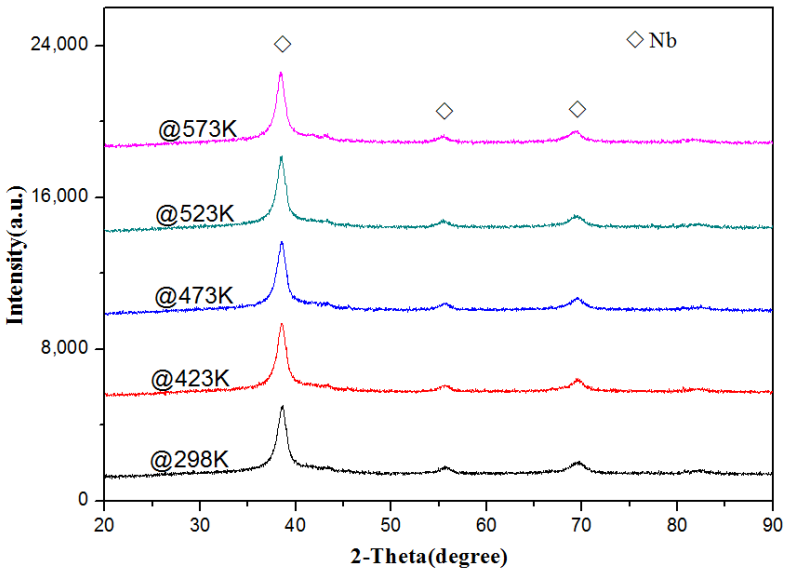


Figure 6. XRD patterns of products after heat treatment at different temperatures (from 298 K to 573 K).

After heat treatment from room temperature to 573 K, the XRD patterns showed that the products did not change, and no new diffraction peaks appeared. These results indicated that the crystal structures of the products did not change, and no chemical reaction occurred at below 573 K. The melting point of Sn is below 504.9 K, and Sn will liquify at temperatures above 504.9 K. However, the results obtained after the 573 K heat treatment showed that Sn did not change and turn to liquid, signifying that Sn reacted with the other elements to exist in a new form during high-energy mechanical alloying.

The XRD patterns of the particles after heat treatment from 573 K to 773 K are depicted in Figure 7. The shapes of the peak diffraction were nearly identical from 573 K to 723 K. After heat treatment temperature increased to 773 K, small diffraction peaks of Nb_3Sn appeared. This finding indicated that reactions that produced Nb_3Sn started when the temperature was above 773 K. Simultaneously, the diffraction peaks of Nb began to fade due to the reaction of Nb with Sn or Sn compounds.

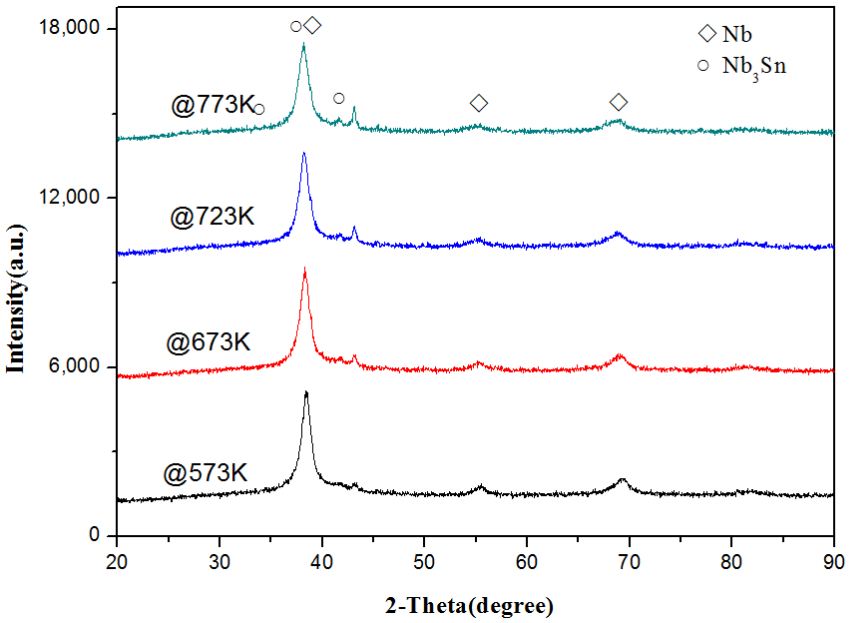


Figure 7. XRD patterns of the products after heat treatment at different temperatures (from 573 K to 773 K).

As shown in Figure 8, Nb diffraction peaks gradually attenuated after heat treatment from 773 K to 903 K. Nb diffraction peaks nearly disappeared at temperatures above 903 K. In this process, Nb_3Sn was produced with increasing temperature. After heat treatment at 903 K, Nb_3Sn phase diffraction peaks became highly apparent. Thus, through high-energy mechanical alloying, the as-milled particles should be at least exposed to an environment with a temperature of above 903 K.

To determine the optimum temperature range of heat treatment, temperatures of 903 K, 913 K, and 923 K were selected to study the crystal structure of the products. As shown in Figure 9, the crystal structures were nearly identical at different temperatures, and Nb_3Sn and NbO_2 diffraction peaks were observed. Nb_3Sn diffraction peaks exhibited slightly higher intensity with increasing temperature.

As shown in Figure 10, the samples were heat treated at different temperatures of 923 K, 933 K, and 943 K. The results indicated that the locations of the diffraction peaks did not change, and no new structures appeared. Thus, the temperature of 923 K was selected to obtain the final Nb_3Sn product.

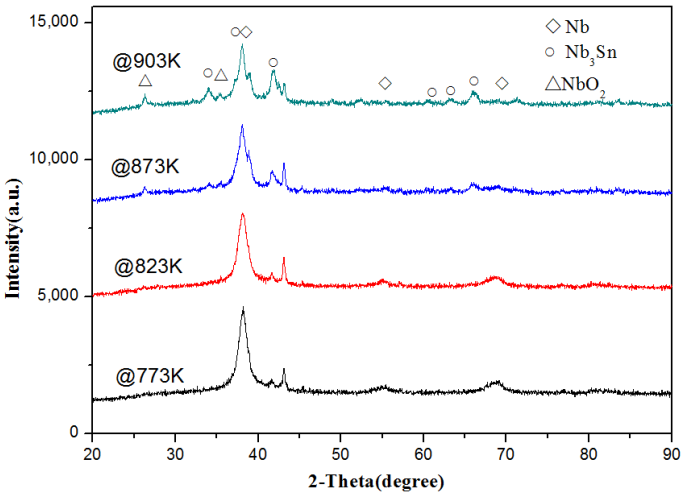


Figure 8. XRD patterns of the products after heat treatment at different temperatures (from 773 K to 903 K).

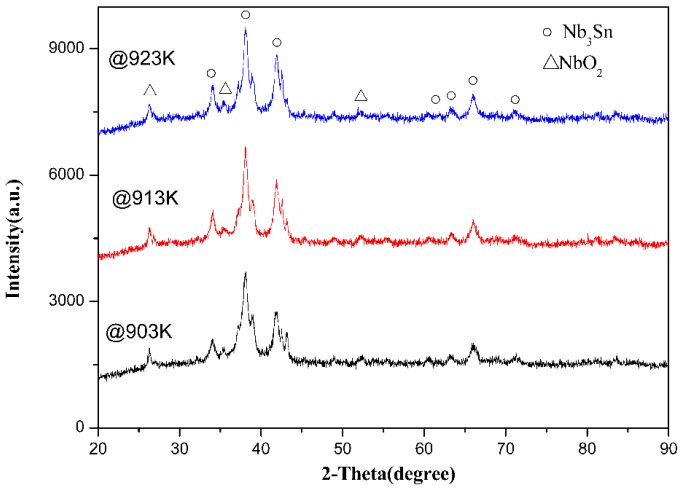


Figure 9. XRD patterns of the products after heat treatment at different temperatures (from 903 K to 923 K).

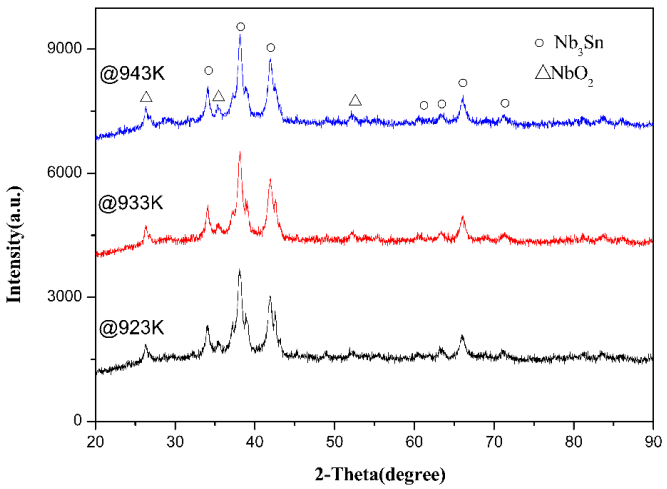


Figure 10. XRD patterns of the products after heat treatment at different temperatures (from 923 K to 943 K).

The effect of higher heat treatment temperatures was studied to determine whether the crystal structure of the product changed when exposed to higher temperatures. Figure 11 shows the XRD patterns of the products after heat treatment at different temperatures ranging from 953 K to 1073 K. The results showed that the diffraction peaks of Nb_3Sn did not change when exposed to temperatures above 973 K, but other impurities, such as Nb_2O_5, appeared. Thus, as-milled particles should not be utilized at above 973 K.

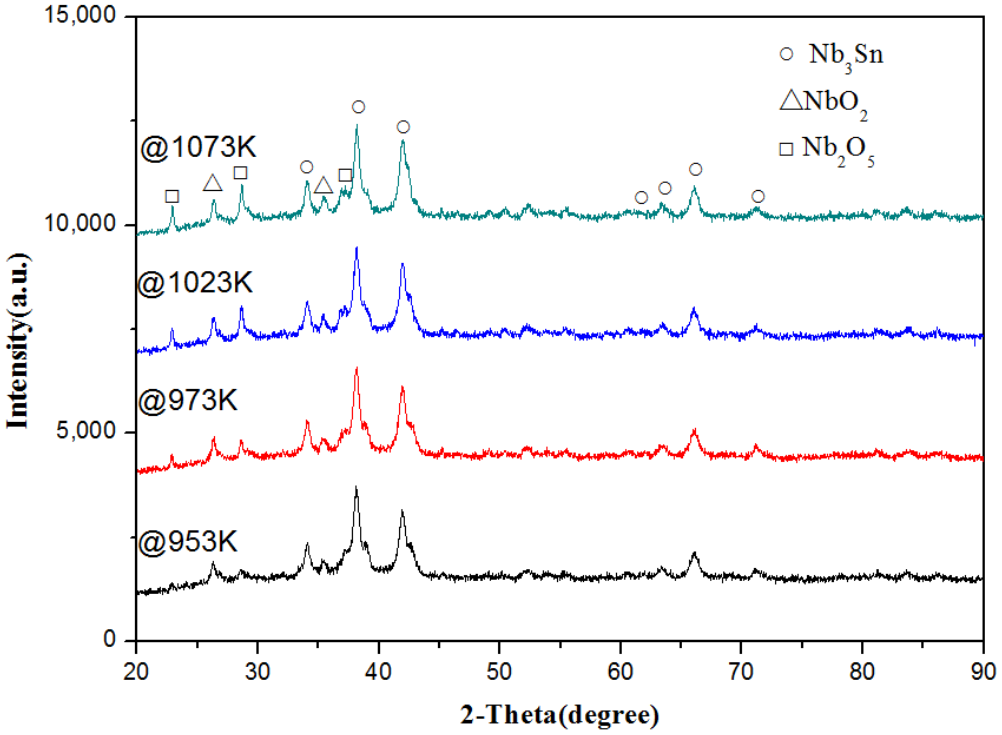


Figure 11. XRD patterns of the products after heat treatment at different temperatures (from 953 K to 1073 K).

The key temperature points of Nb_3Sn heat treatment were presented to show the change in crystal structure during the heat treatment process. As illustrated in Figure 12, the phase transition process from room temperature to 903 K and then to 1073 K was as follows: the original materials of Nb, Sn, and Cu at 298 K exhibited broadened Nb diffraction peaks at 298 K after mechanical alloying. Then, Nb_3Sn and NbO_2 diffraction peaks appeared at 903 K. Finally, Nb_3Sn, NbO_2, and Nb_2O_3 diffraction peaks appeared at 1073 K. In accordance with the solid-state diffusion reaction, different temperatures correspond to different activation energies of atomic diffusion, affecting the diffusion reaction speed and whether diffusion reaction can occur. In accordance with the result of heat treatment, the as-milled particles should be exposed to temperatures above 903 K. However, when the temperature reached 1073 K, diffraction peaks of impurities appeared.

To maximize the Nb_3Sn area, heat treatment time must last for a long time (50–200 h) at high temperature in Nb_3Sn formation reaction. The researchers investigated the effects of reaction time (24–150 h) on the superconducting characteristics of Nb_3Sn. They determined that a 24 h final reaction reached >90% of the highest obtained J_c [18]. To obtain a short reaction time and good performance, the experimental sample received a final reaction for 24 h at 923 K. With this scheme, we can combine the technologies of Nb_3Sn bulk and conductors to fabricate Nb_3Sn superconducting joints on magnets in the future.

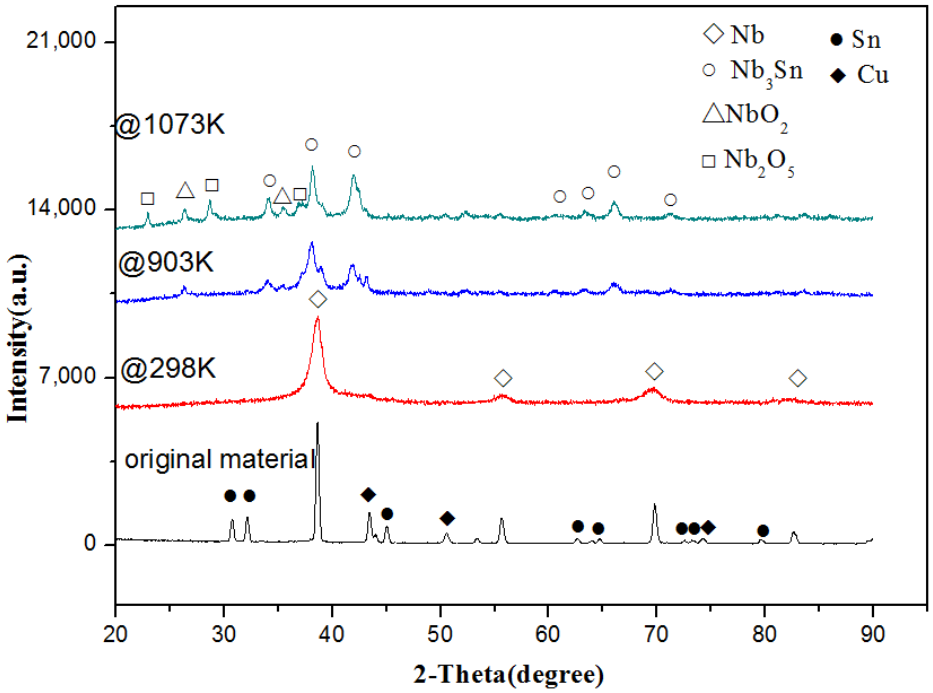


Figure 12. XRD patterns of the products after heat treatment at different temperatures (from 298 K to 1073 K).

Figure 13 shows MT curves of the samples that were ball milled for 5 h and heat treated for 24 h and 50 h. The onset T_c of the samples was between 17 K and 18 K. The T_c value was determined by taking the first deviation point from the linearity that signified the transition from the normal state to the superconducting state. As shown in Figure 13, the transitions of all the samples were relatively steep, indicating that the Nb_3Sn phase formation qualities of the samples were good. The differences among the prepared samples and between the experiment results and the theoretical value may be attributed to the purity of the products. Critical temperature exhibits a relationship with the concentration of Sn and the stoichiometric ratio of Nb and Sn. After high-energy mechanical alloying, the size of Nb and Sn particles sharply decreased. The distribution of Nb and Sn became more unique, and the solid-state diffusion reaction of Nb and Sn occurred on the basis of a more precise stoichiometric ratio of 3:1. $B_{c2}(0)$ can be calculated using the following equation based on the Werthamer–Helfand–Hohenberg theory [19]:

$$B_{c2}(0) = -0.69 T_c \left.\frac{\partial B_{c2}}{\partial T}\right|_{T_c}$$

where B_{c2} is the upper critical magnetic field, T_c is the critical temperature of a Type II superconductor (Nb_3Sn), and 0.69 is the pre-factor constant for the dirty limit [20].

The results led to the conclusion that the $B_{c2}(0)$ of the prepared samples did not appear to depend on the heat treatment time of the samples.

Figure 14 shows the field independence of the critical current density J_c of the heat-treated bulk for 24 h. The heat-treated bulk was about 3 mm in length, 2 mm in width, and 1 mm in thickness. The magnetic J_c was calculated from the magnetization loops based on the critical Bean model [21], as follows:

$$J_c = \frac{\Delta M}{a\left(1 - \frac{a}{3b}\right)},$$

where a and b ($b \geq a$) are the width and length of the sample, respectively.

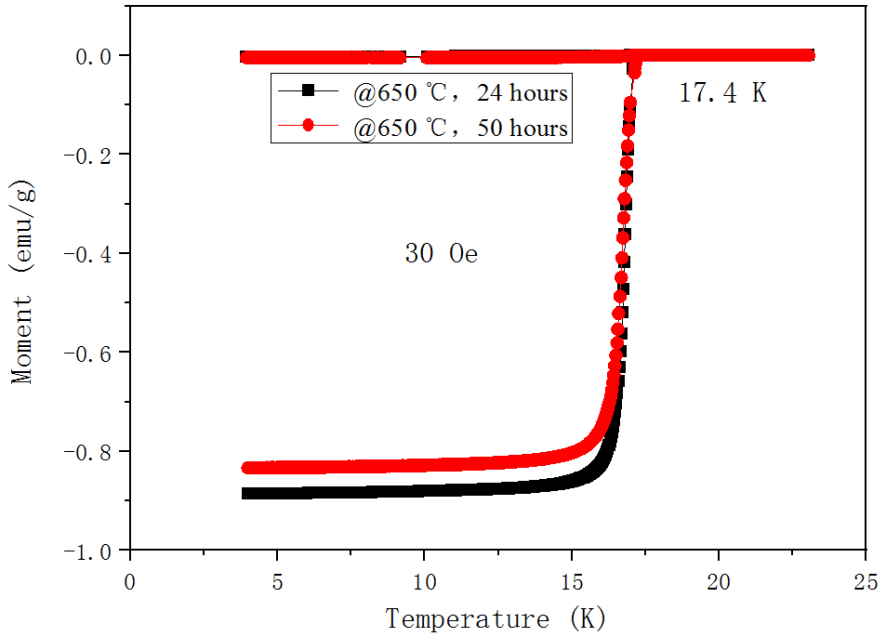


Figure 13. MT curve of the samples that were heat treated for 24 h and 50 h.

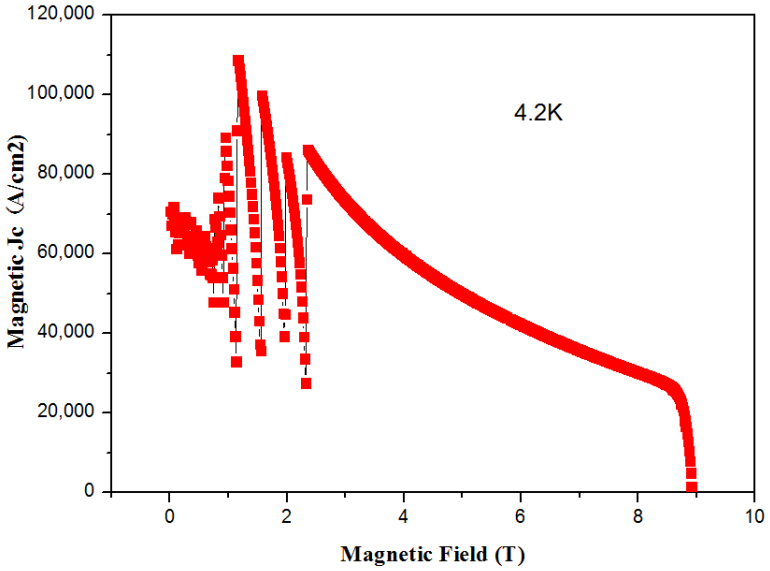


Figure 14. Magnetic critical current density of the sample vs. applied magnetic field at 4.2 K.

J_c decreased with increasing magnetic fields. The phenomenon of the curve in the low magnetic field is attributed to the flux jump, which typically occurs in Nb_3Sn materials at low fields in changing magnetic fields. Flux jumps result in the transition between the superconducting and normal states, which has been readily observed during V–H measurements. Compared with the performance of Nb_3Sn in low magnetic field, we are more concerned about the performance of Nb_3Sn in a high magnetic field, because the Nb_3Sn material will contribute more to the high magnetic field region. As shown in the figure, the magnetic J_c was approximately 30,000 A/cm^2 under 8 T. Considering the limit of the magnetic field in the PPMS instrument (±9 T), the J_c value under 8 T was used to evaluate the performance of Nb_3Sn. The technology can be used for fabricating Nb_3Sn joints in Nb_3Sn magnets. The magnetic intensity in the region of Nb_3Sn joints is lower than that in the center of the magnet. The result can help magnet designers place the Nb_3Sn joint on the location where the joint has no problem to work under such a magnetic field.

4. Conclusions

This study presented the process of Nb_3Sn phase transitions during heat treatment. Nb_3Sn was prepared by heat treating the precursors, which were mechanically alloyed first. The size and crystal structure of the products changed after mechanical alloying for some time. The TEM results indicated that the products exhibited poor crystallinity after ball milling, and this finding was consistent with the XRD results. In accordance with the XRD analysis, the diffraction peaks of Cu and Sn became weaker with increasing ball milling time, and only Nb diffraction peaks were observed after 3 h. The precursors were heat treated from room temperature to 1073 K, and simultaneously, the crystal structures were monitored after exposure to different temperatures. When the temperature was above 773 K during heat treatment, Nb_3Sn began to appear. When the temperature was above 973 K, some impurities, such as Nb_2O_5, appeared. Thus, the heat treatment temperature of the as-milled particles should not be above 973 K. The critical temperatures of the samples that were heat treated at different times were between 17 K and 18 K. The magnetic critical current density of the sample versus the applied magnetic field at 4.2 K illustrated that magnetic J_c was approximately 30,000 A/cm^2 under 8 T. The result can be applied to the fabrication of Nb_3Sn superconducting joints in the future and help magnet designers place the joint in an appropriate location where the joint will not be affected by magnetic intensity.

Author Contributions: Conceptualization, W.S. and S.C.; methodology, W.S.; software, W.S.; validation, W.S.; formal analysis, W.S.; investigation, W.S.; resources, W.S. and S.C.; data curation, W.S.; writing—original draft preparation, W.S.; supervision, S.C.; project administration, S.C. All authors have read and agreed to the published version of the manuscript.

Funding: This research received no external funding.

Data Availability Statement: The authors confirm that the data supporting the findings of this study are available within the article.

Conflicts of Interest: The authors declare no conflict of interest.

References

1. Matthias, B.; Geballe, T.; Geller, S.; Corenzwit, E. Superconductivity of Nb_3Sn. *Phys. Rev.* **1954**, *95*, 1435. [CrossRef]
2. Baig, T.; Yao, Z.; Doll, D.; Tomsic, M.; Martens, M. Conduction cooled magnet design for 1.5 T, 3.0 T and 7.0 T MRI systems. *Supercond. Sci. Technol.* **2014**, *27*, 125012. [CrossRef]
3. Iwasa, Y.; Bascuñán, J.; Hahn, S.; Park, D.K. Solid-Cryogen Cooling Technique for Superconducting Magnets of NMR and MRI. *Phys. Procedia* **2012**, *36*, 1348–1353. [CrossRef]
4. Godeke, A.; Hellman, F.; Kate, H.H.J.T.; Mentink, M.G.T. Fundamental origin of the large impact of strain on superconducting Nb_3Sn. *Supercond. Sci. Technol.* **2018**, *31*, 105011. [CrossRef]
5. Iwaki, G.; Sato, J.; Inaba, S.; Kikuchi, K. Development of bronze-processed Nb_3Sn superconducting wires for high field magnets. *IEEE Trans. Appl. Supercond.* **2002**, *12*, 1045–1048. [CrossRef]
6. Miyazaki, T.; Kato, H.; Hase, T.; Hamada, M.; Murakami, Y.; Itoh, K.; Kiyoshi, T.; Wada, H. Development of High Sn Content Bronze Processed Nb_3Sn Superconducting Wire for High Field Magnets. *IEEE Trans. Appl. Supercond.* **2004**, *14*, 975–978. [CrossRef]
7. Gregory, E.; Pyon, T. Internal tin Nb_3Sn conductor development for high energy physics applications. *Aip Conf. Proc.* **2002**, *614*, 958–967.
8. Lu, X.F.; Hampshire, D.P. The field, temperature and strain dependence of the critical current density of a powder-in-tube Nb_3Sn superconducting strand. *Supercond. Sci. Technol.* **2010**, *23*, 025002. [CrossRef]
9. Di Michiel, M.; Scheuerlein, C. Phase transformations during the reaction heat treatment of powder-in-tube Nb_3Sn superconductors. *Supercond. Sci. Technol.* **2007**, *20*, 55–58. [CrossRef]
10. Xu, X. A review and prospects for Nb_3Sn superconductor development. *Supercond. Sci. Technol.* **2017**, *30*, 093001. [CrossRef]
11. Di Michiel, M.; Scheuerlein, C. Phase transformations during the reaction heat treatment of Nb_3Sn superconductors. *J. Phys. Conf.* **2010**, *234*, 022032. [CrossRef]
12. Oh, S.; Park, S.H.; Lee, C.; Choi, H.; Kim, K. Heat treatment effect on the strain dependence of the critical current for an internal-tin processed Nb_3Sn strand. *Physical C* **2010**, *470*, 129–133. [CrossRef]
13. Zhang, K.; Zhang, P.X.; Shi, Y.G.; Liu, J.W.; Gao, H.X.; Jia, J.J.; Guo, J.H.; Li, J.F.; Liu, X.H.; Feng, Y. An Investigation Into the Heat Treatment Tolerance of WST Nb_3Sn Strands Produced for Massive Fusion Coils. *IEEE Trans. Appl. Supercond.* **2015**, *25*, 1–6. [CrossRef]

14. Lee, J.; Posen, S.; Mao, Z.; Trenikhina, Y.; He, K.; Hall, D.L.; Liepe, M.; Seidman, D.N. Atomic scale analysis of Nb_3Sn on Nb prepared by a vapor-diffusion process for superconducting radiofrequency cavity applications. *arXiv* **2019**, *32*, 024001.
15. Godeke, A. A review of the properties of Nb_3Sn and their variation with A15 composition, morphology and strain state. *Supercond. Sci. Technol.* **2006**, *19*, 68–80. [CrossRef]
16. Patankar, S.N.; Froes, F.H. Formation of Nb_3Sn Using Mechanically Alloyed Nb—Sn Powder. *Solid State Sci.* **2004**, *6*, 887–890. [CrossRef]
17. Menary, M.A.; Menary, M.A. The Effect of Mechanical Alloying on the Structural and Superconducting Properties of Nb_3Sn. 2005, Volume 27, pp. 3–7. Available online: https://www.mendeley.com/catalogue/24a95fbb-8978-3aaa-991e-66b759e6088e/ (accessed on 23 February 2023).
18. Ghosh, A.K.; Sperry, E.A.; Cooley, L.D.; Moodenbaugh, A.M.; Sabatini, R.L.; Wright, J.L. Dynamic stability threshold in high-performance internal-tin Nb_3Sn superconductors for high field magnets. *Supercond. Sci. Technol.* **2004**, *18*, 5–8. [CrossRef]
19. Helfand, E.; Werthamer, N.R. Temperature and Purity Dependence of the Superconducting Critical Field, Hc_2. *Phys. Rev. Lett.* **1964**, *13*, 686–688. [CrossRef]
20. Rekaby, M.; Awad, R.; Abou-Aly, A.I.; Yousry, M. AC Magnetic Susceptibility of $Y_3Ba_5Cu_8O_{18}$ Substituted by Nd^{3+} and Ca^{2+} Ions. *J. Supercond. Nov. Magn.* **2019**, *32*, 3483–3494. [CrossRef]
21. Bean, C.P. Magnetization of High-Field Superconductors. *Rev. Mod. Phys.* **1964**, *36*, 886–901. [CrossRef]

Disclaimer/Publisher's Note: The statements, opinions and data contained in all publications are solely those of the individual author(s) and contributor(s) and not of MDPI and/or the editor(s). MDPI and/or the editor(s) disclaim responsibility for any injury to people or property resulting from any ideas, methods, instructions or products referred to in the content.